

Optical Energy Transport and Interactions between the Excitations in a Coumarin–Perylene Bisimide Dendrimer

Ramūnas Augulis,[§] Audrius Pugžlys,^{§,†} Johannes H. Hurenkamp,^{||} Ben L. Feringa,^{||} Jan H. van Esch,^{‡,||} and Paul H. M. van Loosdrecht^{*,§}

Zernike Institute for Advanced Materials, University of Groningen, Nijenborgh 4, 9747AG Groningen, the Netherlands, and Stratingh Institute for Chemistry, University of Groningen, Nijenborgh 4, 9747 AG Groningen, The Netherlands

Received: July 12, 2007; In Final Form: September 13, 2007

Energy transfer properties of novel coumarin–perylene bisimide dendrimer are studied by means of steady state and time-resolved UV/vis spectroscopy. At low donor excitation density fast (transfer rate ~ 10 ps⁻¹) and efficient (quantum yield $\sim 99.5\%$) donor–acceptor energy transfer is observed. The random distributions of donor–acceptor orientations and distances result in nonexponential energy transfer kinetics. The energy transfer remains independent of excitation density up to densities corresponding to one absorbed photon per 10 dendrimer molecules. At higher excitation densities the transfer rate is found to increase due to excitation of multiple donors per dendrimer. Control of the donor–acceptor energy transfer rate is achieved by pre-excitation of the acceptor and monitored by prepump–pump–probe experiments, which show that the energy transfer rate can be decreased by a factor of 2. The relative orientations of transition dipole moments in the donor and acceptor molecules are found to be one of the key factors determining the energy transfer dynamics at high excitation densities.

I. Introduction

Dendrimers are well-defined branched macromolecules with a high degree of order. The distinctive structure of dendrimers allows encapsulation of active components,^{1–4} which is an important issue in drug delivery,^{5,6} catalysis of chemical reactions,^{7–10} surface modification,^{11–14} and molecular optoelectronics.^{15–17} Over the past decade extensive studies of the optical properties and applications of dendrimers have been carried out. Kawa and Fréchet^{18,19} have employed dendrimeric encapsulation to isolate lanthanide ions from the solvent, leading to a significant suppression of vibrational quenching of the lanthanide luminescence. Dendritic systems are considered as promising candidates for light harvesting and excitation energy transport.^{17,20–29} Efficient light harvesting in dendrimers is realized through a large number of energy donors branching around a single or a few acceptors. The distance between the donors and the acceptors can be optimized for efficient dipole–dipole interaction and Förster energy transfer. In such systems a high UV/vis absorptivity of a large number of donors is potentially beneficial for light harvesting when efficient energy transport takes place. This assures a high-energy flux to the acceptor (or the core of the dendrimer).^{17,29,31–34} A detailed model of donor–acceptor population dynamics, based on a system of differential rate equations, for a first generation dendrimer has been presented in ref 31. For higher generation dendrimers, the light harvesting can be improved through the use of cascade systems containing several different chromophores.^{35–38} Recently, novel energy harvesting and transfer related phenomena in dendrimers, such as photocatalysis^{39,40} and energy

upconversion,^{41,42} have been reported, highlighting the importance of a fundamental understanding of the energy transfer (ET) mechanisms that take place in dendrimeric systems.

Due to the presence of multiple donors per dendrimer, more than one donor per dendrimer can be excited, already at moderate excitation densities. This leads to interactions between the excitations, which potentially can either increase or decrease the ET efficiency. For example Neuwahl et al.,⁴³ while measuring pump–probe spectra in a donor–acceptor-type system at relatively high irradiation intensities, observed residual emission from the donor at delays, which are long compared to the energy transfer time. The phenomenon was explained by proposing that once the acceptor is excited via excitation transfer from one donor molecule ET from the other donors is prohibited. Later on, the effect of donor–acceptor ET restriction when the acceptor is excited was extensively studied by De Schryver and co-workers,^{29,36,37} attributing the phenomena to “exciton blockade”. In contrast, no change in the ET rate upon increasing excitation density was observed by Hania et al. in a coumarin–porphyrin dendrimer.³¹ It was demonstrated that both the difference between the energy transfer rate constants to single and doubly excited acceptor states and the rate of radiationless decay from such doubly excited states are the key parameters determining the overall ET dynamics at high excitation density conditions. A recent paper by Melnikov et al.²⁸ studies the phenomena of simultaneous emission from both donor and acceptor chromophores in a peryleneimide–tetryleneimide dendrimer at the single-molecule level. Though the “exciton blockade” effect would be the most straightforward explanation for the phenomena observed, the authors conclude that additional conditions are necessary, in particular unfavorable donor–acceptor transition orientation and photobleaching of the donors with favorable orientations.

Here, we present detailed studies of the ET properties of a first generation dendrimer composed of four equivalent coumarin

* Author to whom correspondence should be addressed. E-mail: P.H.M.van.Loosdrecht@rug.nl.

† Present address: Photonics Institute, Vienna University of Technology, Gusshausstrasse 27/387, 1040 Vienna, Austria.

‡ Present address: Delft ChemTech, Technical University Delft, Julianalaan 136, 2628 BL Delft, The Netherlands.

§ Zernike Institute for Advanced Materials.

|| Stratingh Institute for Chemistry.

donors surrounding a perylene-bisimide-based acceptor, under both low and high excitation density conditions. Well-defined properties of the coumarins (donor chromophores) and extensively studied perylene bisimide derivatives (acceptor chromophore)^{44–46} as well as high photostability make this dendrimer an excellent model system for studying the interactions between the excitations. An additional advantage of this dendrimer as a model system for ET studies is the difference in the rates of various ET and energy relaxation processes, such as donor–acceptor ET, donor–donor energy hopping, relaxation of the acceptor from the higher excited states to the lowest excited state, and relaxation of both chromophores to the ground state.

Time-resolved fluorescence and intensity dependent pump–probe techniques are employed to study the excitation dynamics. In addition, control of donor–acceptor energy transfer is achieved through pre-excitation of the acceptor using multicolor prepump–pump–probe techniques. These experiments show that the energy transfer rate can be reduced by a factor of 2. One of the key factors determining the ET rate at high fluence is the relative orientation of the transition dipole moments in the donors and the acceptor, which exceeds the influence of spectral overlap changes in the dendrimer. In addition, by performing molecular dynamics (MD) simulations, we have studied the influence of the flexible nature of the dendrimer on the ET dynamics.

The paper is organized as follows. After the introduction of the experimental procedures (section II) we start in section III.1 with a discussion on the qualitative properties of the ET in the first generation coumarin–perylene bisimide dendrimer. The ET dynamics studied by time-resolved measurements at low excitation densities are discussed in section III.2. Analytical considerations and experimental confirmation concerning interactions between excitations at high excitation densities are presented in sections III.3 and III.4, respectively. In section III.5 the results of optical prepump–pump–probe experiments are presented, which allow distinctive investigation of the effect of an excited acceptor on the ET rate.

II. Materials and Methods

The coumarin–perylene bisimide dendrimer (C4P) (Figure 1c) consists of four coumarin subunits acting as energy donors and a single perylene bisimide core, which is connected to the donors via spacers. Model constituent compounds are also shown in Figures 1a and 1b: (a) two donors connected via a spacer and (b) a perylene bisimide acceptor with two spacers. The synthesis of C4P and constituent compounds was performed using an amide coupling methodology. The details of the synthesis will be discussed elsewhere.⁴⁷ Analytical data (¹H and ¹³C NMR and mass spectrometry (MALDI-TOF)) for the C4P and constituent compounds are in agreement with the structures shown. All optical experiments were carried out at room temperature under ambient air conditions with the compounds dissolved in chloroform.

Energy transfer dynamics in C4P were studied by means of time-resolved fluorescence and transient absorption (pump–probe) spectroscopy. To study interactions between excitations, pump–probe measurements were carried out at different excitation densities. In addition, prepump–pump–probe experiments, which potentially disclose a dependence of the ET dynamics on the population of acceptor sites, were performed.

Time and spectrally resolved (spectral resolution is ca. 0.6 nm) fluorescence measurements were performed using a streak camera system with a synchroscan sweep unit (Hamamatsu). The sample was irradiated by the frequency-tripled ($\lambda = 325$

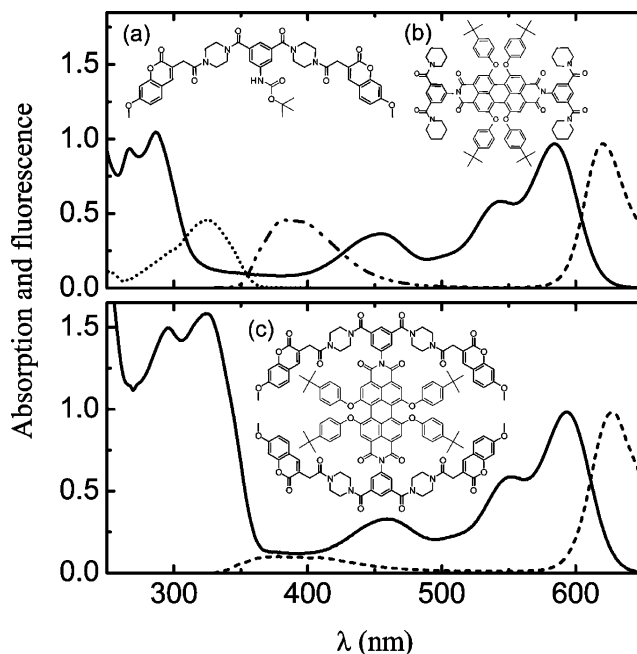


Figure 1. Top panel: Absorption and fluorescence spectra of donor (absorption, dotted line; fluorescence, dash–dotted line) and acceptor (absorption, solid line; fluorescence, dashed line) constituents. The chemical structure of the constituent compounds is shown in the insets: (a) Two donors attached to a spacer and (b) an acceptor with two spacers attached. Bottom panel: Absorption and fluorescence spectra of the C4P dendrimer (absorption, solid line; fluorescence, dashed line). (c) The chemical structure of the C4P dendrimer is shown in inset. All absorption data are presented in absolute units of optical density. Spectra are measured in a 2 mm cell at concentration of 10^{-4} M for all compounds. Fluorescence spectra are scaled to the maxima of corresponding absorption bands.

nm, $\tau = 120$ fs) output of a tunable 76 MHz Ti:sapphire laser (Mira 900, Coherent), which was pumped by an all-solid-state diode-pumped, frequency-doubled Nd:YVO₄ laser (Verdi, Coherent). A pulse picker was used to reduce the repetition rate to 1.9 MHz. To preserve low excitation density conditions the pulse energy was attenuated to 1 pJ, which corresponds to one photon absorbed per 10^5 donor molecules per pulse. The time resolution of the experiments, as determined by recording scattered light from the excitation pulse was 7 ps. To avoid population of the acceptor triplet states by multiple laser pulses and to ensure photostability of the sample, a 10^{-4} M solution of C4P in CHCl₃ was pumped along a 0.5 mm fused silica cell by a peristaltic pump. The absorption spectra of the samples measured before and after the time-resolved fluorescence experiments were identical, which indicates the absence of photodecomposition.

Pump–probe experiments were performed in a standard geometry using two independently tunable noncollinearly pumped optical parametric amplifiers (NOPAs) (Topas White, Light Conversion) as pump and probe sources. The NOPAs were pumped by a Ti:sapphire laser/regenerative amplifier system (Hurricane, Spectra Physics) producing 120 fs, 800 nm pulses at 1 kHz repetition rates. The sample was excited at 325 nm, corresponding to the absorption maximum of the donor molecule. UV pulses at 325 nm were obtained by frequency doubling of the 650 nm signal wave of one of the NOPAs in a 0.15 mm β -barium borate (BBO) crystal and subsequent compressing in a double-pass compressor based on two fused silica prisms. In addition to the pulse shortening, the compressor allows for spatial separation of the fundamental and second harmonic beams. The time

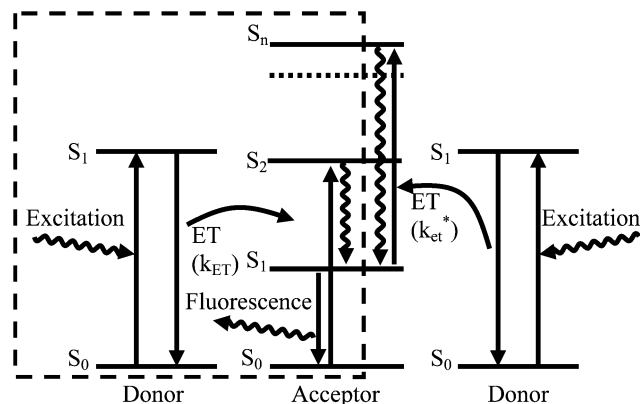


Figure 2. Energy transfer diagram showing the ET processes where one donor per dendrimer is excited (boxed part) and where two donors per dendrimer are excited (full diagram).

resolution of pump–probe experiments, as measured by monitoring two-color two-photon absorption in a 100 μm glass plate, was 70 fs. For the measurements of the dynamics of the pump–probe spectrum, white light in a 390–800 nm spectral range was generated in a 1 cm water cell. The time resolution in this case was lower because of the chirped white light, though it remains in a sub-picosecond range.

Prepump–pump–probe experiments were performed by pre-exciting acceptors with a high-energy prepump pulse centered at $\lambda_{\text{prep}} = 550$ nm. Then after a time delay a pump pulse at wavelength $\lambda_{\text{ex}} = 325$ nm, again corresponding to the maximum of the donor absorption, was applied. The third pulse centered at wavelength $\lambda_{\text{pr}} = 325$ nm probed the photoinduced optical density changes in the C4P dendrimers. The delay between prepump and pump pulses was variable in a 1 ns time window. Polarization of the prepump pulse was either parallel or perpendicular to the polarization of the pump pulse.

Molecular dynamics simulations at room temperature were performed using the Langevin MD method with MM+ force field (Hyperchem 7.5) in a medium with a viscosity of chloroform (5.8×10^{-4} N s m^{-2}) at room temperature. Simulations were performed on a single dendrimer molecule with no solvent molecules present. Data were collected for 10 ns with a 100 fs time step after 1 ns of equilibration time, while atom positions were updated every 1 fs.

III. Results and Discussion

III.1. Donor–Acceptor ET in C4P: Qualitative Description. The realization of both efficient light energy harvesting and transport requires a rather weak interaction between donors and between donor and acceptor units as well as sufficient spectral overlap of donor and acceptor resonances, i.e., donor fluorescence and acceptor absorption. To estimate the interactions between the constituent parts of the C4P dendrimer, to confirm the occurrence of donor–acceptor ET, and to qualitatively examine ET properties, we measured steady state absorption and fluorescence spectra of the model compounds and compared them with the ones characteristic for the whole dendrimer.

Steady state absorption and fluorescence spectra of donor and acceptor constituents are presented in the top panel of Figure 1. A simplified energy level diagram of C4P, which also shows a number of possible transitions, is shown in Figure 2. The absorption spectrum of the donor molecule is dominated by a single band centered at around 325 nm, which originates from the $S_0 \rightarrow S_1$ transition. The corresponding fluorescence spectrum

consists of a band centered at 385 nm. The absorption spectrum of the acceptor molecule in the visible spectral region is characterized by a $S_0 \rightarrow S_1$ transition leading to an absorption band peaking at 584 nm featuring a vibronic progression as well as by a $S_0 \rightarrow S_2$ transition resulting in an absorption band with a maximum at 455 nm. The fluorescence spectrum of the acceptor has a maximum at 620 nm and is a mirror image of the $S_0 \rightarrow S_1$ absorption band. As can be seen from the upper panel in Figure 1, the $S_0 \rightarrow S_2$ absorption band of the acceptor overlaps partially with the fluorescence band of the donor enabling resonant ET. The fluorescence spectrum of the complete dendrimer (Figure 1, lower panel), measured while exciting at the absorption maximum of the donors (325 nm), shows clearly the occurrence of donor–acceptor ET: The fluorescence of the donors is quenched significantly, while the fluorescence intensity of the acceptor is increased considerably.

The absorption spectrum of the dendrimer (lower panel of Figure 1) is red-shifted by ca. 100 cm^{-1} with respect to the weighted sum of absorption spectra of donors and acceptor with spacer, indicating that donor–acceptor interaction is rather weak. The weakness of the interaction allows for a description of the ET dynamics in terms of the dipole–dipole Förster energy transfer theory. A more detailed analysis of the changes in the C4P absorption spectrum due to attachment of different constituents is discussed in ref 47.

Finally, the linear donor and acceptor spectra shown in Figure 1 overlap partially. This makes selective excitation of donor molecules impossible. Nevertheless, by taking into account that the dendrimer is composed of four donors and a single acceptor, we estimate that the selectivity toward donor excitation is still about 85% at 325 nm.

For more evident verification of the ET, time-resolved fluorescence measurements were performed. The experiments reveal a single-exponential decay of excitations for both constituent parts of the dendrimer with decay time constants of 2.1 and 6.7 ns for the donor and acceptor model compounds (Figures 1a and 1b), respectively (results are not shown). The decay time constants obtained are close to those reported for similar dyes,^{48,49} indicating that the chemical modifications of the chromophores do not alter the photophysical properties of the compounds considerably. In addition, the measured fluorescence quantum yield for both coumarin and the side branch model compound (Figure 1a) is found to be 70%, indicating that the spacer does not affect the fluorescence efficiency of the donors. The measured emission quantum yields for the acceptor model compound (Figure 1b) and for the whole dendrimer (Figure 1c) are 92% and 85%, respectively, showing that the influence of the incorporation of the acceptor in the dendrimer on the emission efficiency of the acceptor is rather low.

The fluorescence kinetics in a 100 ps time window after excitation of the dendrimer at 325 nm are shown in Figure 3. The wavelengths 385 and 620 nm correspond to the fluorescence maxima of donor and acceptor units, respectively. After deconvolution of the instrumental response, the fluorescence of the dendrimer at 385 nm is found to decay, while the fluorescence at 620 nm features a delayed formation, both with the time constant of about 10 ps. The observed precursor–successor relationship points toward rather efficient (estimated quantum yield is 99.5%) donor–acceptor ET. It appears that the growth of fluorescence of the acceptors is slightly faster than the decay of fluorescence of the donors, which, most likely, originates from direct excitation of ca. 15% of the acceptor molecules. About 4% of the fluorescence of the donor units

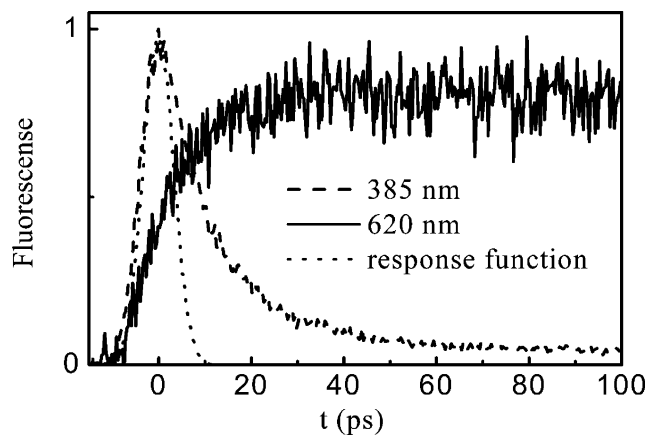


Figure 3. Fluorescence decay observed for C4P at wavelengths of $\lambda_{\text{pr}} = 385$ nm (dashed line) and $\lambda_{\text{pr}} = 620$ nm (solid line), corresponding to the maxima of the fluorescence spectra of the donor and the acceptor, respectively. Excitation wavelength is $\lambda_{\text{ex}} = 325$ nm. The system response function is shown by the dotted line.

decays with a time constant of 2.1 ns. Because the 2.1 ns decay time coincides with the excitation lifetime of the side branch model compounds (Figure 1a) and the long time scale emission spectrum matches the emission of donors or side branches, it is most likely that the slow emission component originates from residual, disconnected, donor molecules.

A simple, qualitative diagram of ET in C4P at low excitation energies is depicted in the boxed area of Figure 2. First, an incoming photon excites the donor from S_0 to S_1 . Subsequently ET from donor to acceptor takes place, resulting in an S_2 excited acceptor state, which decays rapidly via a nonradiative $S_2 \rightarrow S_1$ transition to the S_1 state on a ~ 100 fs time scale. Finally, the acceptor decays radiatively from S_1 to S_0 , leading to the fluorescence observed.

III.2. ET at Low Excitation Density. As noted in the previous section, the interaction between the donor and the acceptor chromophores of the dendrimer is weak; therefore the donor–acceptor ET rate constant can be estimated using the Förster dipole–dipole ET model⁵⁰

$$(k_{\text{ET}})^{-1} = (k_{\text{D}})^{-1} \left(\frac{R_{\text{DA}}}{R_0} \right)^6 \quad (1)$$

where R_{DA} is the donor–acceptor distance, k_{ET} and k_{D} are the rate constants for the energy transfer and the donor decay, respectively, and R_0 is the Förster radius

$$R_0^6 = C \frac{\kappa^2 \phi_{\text{D}}}{N_{\text{A}} n^4} J \quad (2)$$

where $J = \int_0^{\infty} I_{\text{D}}(\lambda) \epsilon_{\text{A}}(\lambda) \lambda^4 d\lambda$ in this equation represents the overlap integral of donor fluorescence $I_{\text{D}}(\lambda)$ and acceptor absorption symbolized by the extinction coefficient, $\epsilon_{\text{A}}(\lambda)$, κ^2 is an orientational factor, ϕ_{D} is the fluorescence quantum yield (QY) of a separate donor, N_{A} is Avogadro's number, n is the refractive index of the medium, and $C = 9000(\ln 10)/128\pi^5 \approx 0.53$.

MD simulations give an average distance between the donor and acceptor molecules of $\langle R_{\text{DA}} \rangle = 1.5$ nm. The simulations of the dendrimer geometry show that rotation is rather free around the bonds adjacent to the amide carbonyls. However, the time scale of the structural fluctuations ranges from tens to hundreds of picoseconds. Specifically, donor–acceptor distance autocorrelation decay could be fitted with two exponents with time constants of 56 and 1550 ps. Thus, even the fastest fluctuations

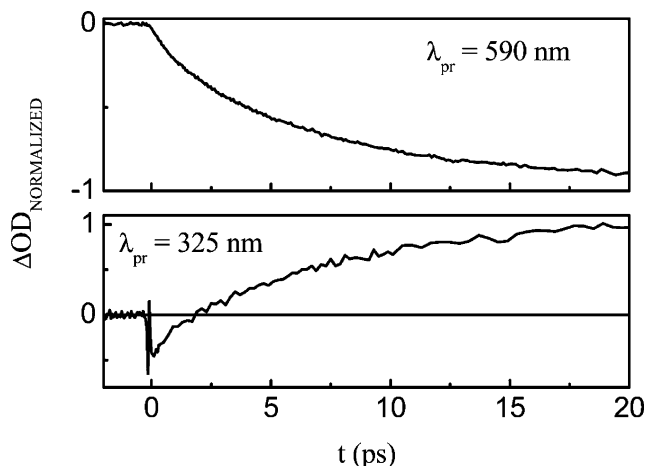


Figure 4. Pump–probe transients normalized to the long time scale signal ($\Delta\text{OD}(t > 100$ ps)), measured after excitation of the C4P dendrimer at $\lambda_{\text{ex}} = 325$ nm. The probe wavelengths of $\lambda_{\text{pr}} = 325$ nm and $\lambda_{\text{pr}} = 590$ nm correspond to the maximum of photoinduced bleaching for the donor and the acceptor, respectively.

are expected to be several times slower than the donor–acceptor ET. Consequently, a solution of dendrimers can be treated as an ensemble of rigid molecules with static structural variations. Assuming a static random distribution of orientations⁵¹ between the transition dipole moments of the donor and acceptor units leads to an orientational factor of $\kappa^2 = 0.845^2 \times 2/3$.⁵² Using the bulk value of the refractive index of chloroform $n = 1.45$, the donor–acceptor distance $\langle R_{\text{DA}} \rangle = 1.5$ nm, the donor fluorescence lifetime $\tau_{\text{D}} = 2.1$ ns and the measured quantum yield $\phi_{\text{D}} = 70\%$, and the overlap integral of $J = 2.33 \times 10^{14} \text{ M}^{-1} \text{ cm}^{-1} \text{ nm}^4$ estimated from the experiments, we obtain an ET time constant of $k_{\text{ET}}^{-1} = 15$ ps.

As is evident from eq 1, the ET rate constant is extremely sensitive to variations of the distance between donor and acceptor units, which, because of the flexible nature of the dendrimer mentioned above, can be distributed over quite a wide range. In addition, donor–acceptor dipole orientations are not completely random, so the estimated κ value is not precise. Another limiting factor for the precision of the calculated ET rate is the finite size of the perylene bisimide and coumarin molecules: The Förster ET model is applicable for point dipoles separated by a specific distance and can substantially fail in describing energy transfer processes when the distance between the chromophores becomes similar to the size of the chromophores.^{53–57} In the case of C4P the donor and acceptor chromophores are relatively large compared to the distances between them; thus an extended dipole approach in calculating the ET rate would be more relevant. Given these limitations the ET rate constant (15 ps) calculated here is in reasonable agreement with that determined experimentally from the time-resolved fluorescence measurements.

Although the time-resolved fluorescence measurements confirm efficient ET in C4P, the time resolution of the streak camera (ca. 7 ps) is insufficient for a detailed examination of the ET dynamics. Time- and frequency-resolved pump–probe experiments with a sub-100 fs time resolution were employed to characterize the ET dynamics more quantitatively. The dendrimers were excited at the wavelength corresponding to the maximum of the donor absorption. Experiments were carried out at a relatively low excitation density corresponding to one photon absorbed per 30 dendrimer molecules.

The pump–probe trace measured at probe wavelengths of 325 nm, corresponding to bleaching of the $S_0 \rightarrow S_1$ donor absorption band and to $S_1 \rightarrow S_n$ photoinduced absorption in the acceptor, is presented in the lower panel of Figure 4. The

bleaching dynamics of the $S_0 \rightarrow S_1$ absorption band in the acceptor at 590 nm are shown in the upper panel of Figure 4. The pump–probe dynamics of the other bands of the acceptor (bleaching at 470 nm and photoinduced absorption above 680 nm) correlate well with the bleaching dynamics of the $S_0 \rightarrow S_1$ band. The band in the vicinity of 590 nm has been chosen for the monitoring of the occupation of the acceptor's S_1 state in all experiments, because of its strong response, thus giving the best signal-to-noise ratio. Although the experiments are performed with a much higher time resolution, the interpretation of the dynamics observed in the pump–probe experiments is not as straightforward as it is for time-resolved fluorescence experiments. The complexity arises from the spectral overlap of pump–probe signals originating from the different photoinduced features in the donor and acceptor units. For instance, in the case of probing at 325 nm (Figure 4, lower panel) bleaching of the donor band is observed directly after excitation. As a result of ET from the donor to the acceptor, this bleaching decays and evolves into photoinduced absorption caused by excited acceptor molecules (see the following section for more details). From the magnitudes of the initial photoinduced bleaching and the photoinduced absorption measured at later times, we estimate a ratio of 0.4 between the contributions of donor and acceptor units to the pump–probe signal. Because after ET from the donor to the acceptor the internal conversion $S_2 \rightarrow S_1$ is very fast (not quite resolvable at the time resolution available), the formation of the photoinduced absorption depicted in the bottom panel of Figure 4 reflects the ET dynamics from the donor to the acceptor.

Analysis of pump–probe transients, such as the ones shown in Figure 4, confirms a precursor–successor relationship as observed in the time-resolved fluorescence experiments and reveals that ET proceeds on a sub-10 ps time scale. However, the dynamics measured show, evidently, nonexponential character resulting from the flexible nature of C4P molecules. In general, the orientation of a donor molecule with respect to the acceptor also affects the ET rate, however, to a lesser extent. Taking only variations of the donor–acceptor distance into account, the ET dynamics $N(t)$ can be modeled in the following way

$$N(t) = \int_0^\infty \frac{1}{\sigma\sqrt{2\pi}} \exp\left(-\frac{(r-1)^2}{2\sigma^2}\right) \exp\left(-\frac{k_{\text{eff}}t}{r^6}\right) dr \quad (3)$$

In this equation, it is assumed that the donor–acceptor distances have a normal distribution with a standard deviation of $\sigma \ll 1$,⁵¹ and k_{eff} is the “effective” ET rate corresponding to that of the mean donor–acceptor distance $\langle R_{\text{DA}} \rangle$. We assume that for every donor–acceptor distance $r = R/\langle R_{\text{DA}} \rangle$ the dynamics are monoexponential with a rate constant determined by the distance only. The combined dynamics are obtained by integrating over the donor–acceptor distance r . We used eq 3 to fit the experimental data presented in the top panel of Figure 4. To emphasize the nonexponentiality of the dynamics, a normalized pump–probe signal subtracted from unity is plotted in Figure 5 in a logarithmic scale. By fitting the experimental data, we obtain $\sigma = 0.105$ and $k_{\text{eff}}^{-1} = 7$ ps. The deviation of the distances σ is in agreement with the range of donor–acceptor distances determined from the MD simulations.

III.3. Analytical Description of ET Dynamics in C4P at High Excitation Densities. Experiments at low excitation density as presented in the previous sections give a consistent picture and understanding of the ET processes in C4P. One important aspect of the ET dynamics, namely, the consequences of multiple excitations on a single C4P dendrimer, has so far not been addressed. Therefore, we have performed pump–probe experiments with high excitation densities (more than 1 photon per dendrimer absorbed). However, before turning to the data,

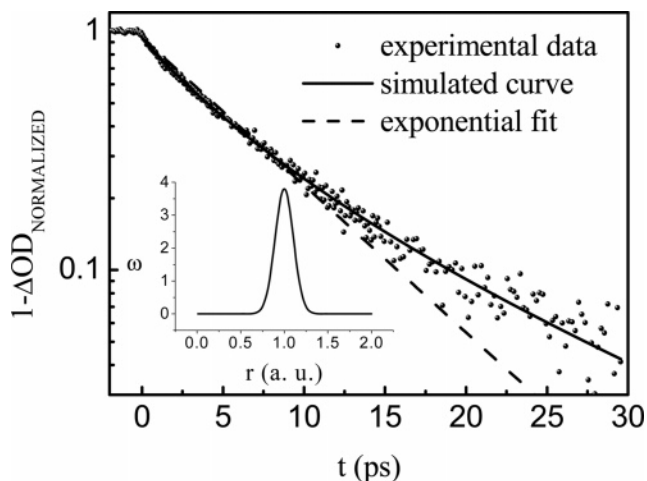


Figure 5. Pump–probe signal at a probe wavelength of $\lambda_{\text{pr}} = 590$ nm recalculated from Figure 4 as explained in the text (dots), single-exponential fit to the data (dashed line), and curve simulated by using eq 3 (solid line). The inset shows the distribution of donor–acceptor distances used in eq 3.

a simple rate model describing ET processes at high excitation densities based on the diagram shown in Figure 2 will be considered, first taking only the effects of multiple donor excitation into account and later also discussing the effects of excitation-induced spectral changes. The diagram shown in Figure 2 reads as follows: First an acceptor is excited via the process described in the previous sections (boxed area); second, before this excited S_1 state decays, another excitation from a second donor reaches the acceptor (right side), and the acceptor is excited from S_1 to some higher state S_n ; third, rapid relaxation of the acceptor back to the S_1 state takes place on a sub-100 fs time scale. As a result, the excitation energy from an additionally excited donor may easily be dissipated nonradiatively. Assuming that ET to an acceptor in the S_0 and S_1 states proceeds with rate constants k_{ET} and k_{ET}^* , respectively (as in Figure 2), one can distinguish two interesting boundary cases: $k_{\text{ET}} \gg k_{\text{ET}}^*$ and $k_{\text{ET}} \ll k_{\text{ET}}^*$. The first case can be considered as an “ET blockade”: Only the energy of one of the excited donors is transferred initially to the acceptor, while the remaining excitation energy is temporarily stored on the other donors (assuming long radiative donor decay times as is the case here) until the acceptor relaxes to the S_0 state. This would be a desirable situation for energy harvesting, because the superfluous absorbed photon energy would be stored until the acceptor is ready to accept a new energy packet. The second case provides “enhanced ET” to the excited acceptor, i.e., overall ET speed up with increasing excitation density. In this case, however, the excess energy absorbed by the donors is lost through nonradiative $S_n \rightarrow S_1$ decay on the acceptor.

The excitation dynamics in C4P, including the interaction of multiple excitations, can be described by a system of differential rate equations³¹

$$\begin{cases} \frac{dN_j}{dt} = -j(k_{\text{D}} + k_{\text{ET}})N_j + (j+1)k_{\text{D}}N_{j+1} + k_{\text{A}}N_j^* \\ \frac{dN_j^*}{dt} = (j+1)k_{\text{ET}}N_{j+1} - (k_{\text{A}} + j(k_{\text{D}} + k_{\text{ET}}^*))N_j^* + \\ (j+1)(k_{\text{D}} + k_{\text{ET}}^*)N_{j+1}^* \end{cases} \quad (4)$$

where the generation terms have been omitted. The index $j = 1, \dots, 4$ in this set of equations represents the number of excited

donor molecules on a single dendrimer. N_j is the number of dendrimers with nonexcited acceptor and j excited donors, whereas N_j^* represents the number of dendrimers with an excited acceptor and again with j excited donors. Note that for C4P only four donors are attached to the acceptor, which is taken into account by setting $N_5 = N_5^* = 0$. k_D and k_A in eq 4 are the donor and acceptor relaxation rates, respectively. k_{ET} and k_{ET}^* are the rates of ET from a donor to an acceptor in the ground state and in the first excited state, respectively.

By describing ET dynamics in this way, it is assumed that the $S_n \rightarrow S_1$ relaxation in this system is much faster than the ET itself and the donor–donor ET is negligible. The first assumption is based on the observation that after excitation of the S_2 state an instantaneous formation of the S_1 population of the acceptor is observed on the time scale of our experiments. The second assumption is reasonable because the donor–donor overlap integral (J in eq 2) is approximately 2 orders of magnitude smaller, while the donor–donor distances are of the same order as donor–acceptor distances. In addition, the anisotropy decay was measured for coumarin and biscoumarin using 325 nm light for the pump and probe. The anisotropy in coumarin was decaying monoexponentially, with a time constant of 81 ps, governed by the rotational motion of the coumarin molecules only. The same measurement for biscoumarin revealed monoexponential decay as well, with a 93 ps time constant. In this case the anisotropy is decaying at a slightly lower rate due to the restricted motion of the interconnected coumarins. If fast donor–donor ET were present in the biscoumarin, then we would expect a faster biexponential decay of anisotropy, as observed in multichromophoric systems when donor–donor energy hopping is present.^{58,59}

The probability of singlet–singlet annihilation in donors when multiple donors are excited cannot be completely excluded, although no fast (on a 100 ps time scale) pump–probe dynamics were observed in biscoumarin at high excitation densities (>1 photon per biscoumarin), so we may safely assume that on the donor–acceptor ET time scale singlet–singlet annihilation is negligible even at high excitation densities. Another process, which we neglect in our model, is the possibility of triplet formation in the coumarins. Because the triplet formation yields in coumarins usually are on the order of several percent,⁶⁰ their formation rates are on the order of at least several nanoseconds and have therefore no influence on the picosecond time scale of donor–acceptor ET dynamics.

If $k_A \ll k_{ET}$ and $k_D \ll k_{ET}$, which is evidently the case for C4P (see section III.1), then the dynamics of the total population of excited donors and acceptors can, according to the eq 4, be expressed as

$$\frac{dN_D}{dt} = \sum_{j=1}^4 \left(\frac{dN_j}{dt} + \frac{dN_j^*}{dt} \right) j = -k_{ET} \sum_{j=1}^4 jN_j - k_{ET}^* \sum_{j=1}^4 jN_j^* \quad (5.1)$$

$$\frac{dN_A}{dt} = \sum_{j=1}^4 \frac{dN_j^*}{dt} = k_{ET} \sum_{j=1}^4 jN_j \quad (5.2)$$

where N_D and N_A are the total numbers of excited donors and acceptors, respectively. Equation 5.2 shows that the dynamics of excitations in acceptors are independent of k_{ET}^* , permitting the study of the effects caused only by the excitation of multiple donors in the same dendrimer. In the case of an “ideal” dendrimer, for which the donor molecules are selectively

excited, the number of acceptor molecules contributing to the signal is

$$N_A|_{t \gg t_{ET}} = \sum_{j=1}^4 N_j \Big|_{t=0}$$

while the contribution of a single dendrimer to the overall signal can be expressed as

$$\frac{dN_A}{dt} \Big|_{t=0} \frac{1}{N_A|_{t \gg t_{ET}}} = \frac{\sum_{j=1}^4 jN_j}{\sum_{j=1}^4 N_j} k_{ET} \quad (6)$$

Equation 6 demonstrates the nonlinearity of the ET dynamics at high excitation densities; i.e., the population of dendrimers with an excited acceptor evolves in time depending on how many donors are excited on a single dendrimer. The right-hand side of eq 6 is relevant to the acceptor population growth rate constant at $t = 0$. In the case of low excitation density, it is simply equal to k_{ET} . At high excitation densities where multiple donors are excited on a dendrimer (N_2, N_3 , and/or $N_4 > 0$) the ET would, based solely on the number of excited donors, speed up.

Apart from the number of excited donors, a change of spectral properties of the acceptor, which occurs as a consequence of the ET process, may also influence the ET dynamics. According to eq 4 under high excitation density conditions when multiple donors in the dendrimer are excited and when internal conversion ($S_n \rightarrow S_1$) in the acceptor is much faster than the ET itself, ET can be understood in a sequential way (see diagram presented in Figure 2). If no structural changes occur in the dendrimer during the first step of ET (static distribution of donor–acceptor distances), then the rate constant of the second ET step would be determined by the spectral properties only, which in eq 2 are taken into account by an overlap integral J . Consequently, the effect of spectral changes to the ET rate can be accounted for by evaluating the differential overlap integral of donor fluorescence and photoinduced acceptor absorption

$$\Delta J = J^* - J = \int_0^\infty F_D(\lambda) \Delta \epsilon_A(\lambda) \lambda^4 d\lambda \quad (7)$$

where $J^* = \int_0^\infty F_D(\lambda) \epsilon_A^*(\lambda) \lambda^4 d\lambda$ in eq 7 is the overlap integral of donor fluorescence with the absorption of the acceptor in the S_1 energy state and $\epsilon_A^*(\lambda)$ is the extinction coefficient of the excited acceptor. As one can see from eq 7 the sign of $\Delta \epsilon_A(\lambda)$ or, in other words, the sign of the optical density changes in the spectral region of the donor fluorescence determines the sign of the change of ET rate, assuming that other factors, such as donor–acceptor distance R_{DA} and geometrical κ factor, remain unchanged. The first assumption seems to hold, because, as discussed in the previous section, the dendrimer geometry hardly changes on the ET time scale. The second assumption might not be accurate because it is not guaranteed that the orientation of the $S_0 \rightarrow S_2$ and $S_1 \rightarrow S_n$ transition dipoles in the acceptor are the same. If these are different, then one has to include different geometrical factors for the different transitions in evaluation of eq 7. Neglecting this point for the moment, eq 7 states that the ET from the donor to the excited acceptor is faster than donor–nonexcited acceptor transfer when $\Delta \epsilon_A(\lambda) > 0$ and slower when $\Delta \epsilon_A(\lambda) < 0$.

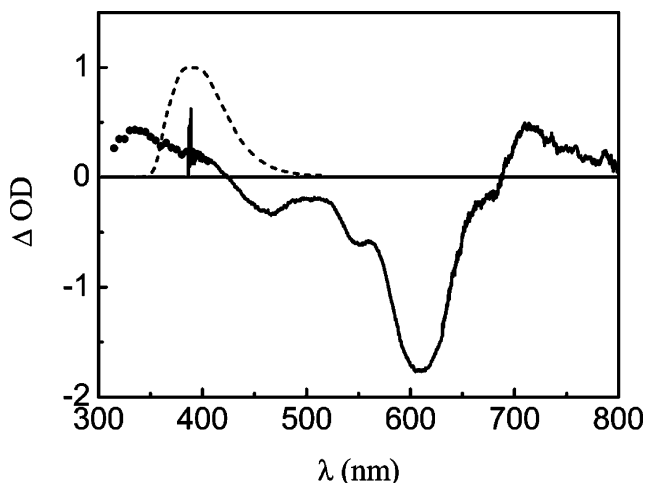


Figure 6. Transient absorption spectrum of the C4P dendrimer at 30 ps after excitation with $\lambda_{\text{ex}} = 325$ nm (solid line) and fluorescence spectrum of the donor molecules (dashed line, same as displayed in Figure 1). Filled circles represent transient absorption data at 30 ps obtained using fixed probe wavelengths. The change in optical density, ΔOD , has been rescaled to match a concentration of 10^{-4} M excited molecules in a 2 mm cell to facilitate comparison to the absorption and fluorescence spectra of Figure 1. (The actual concentration in the experiment was 10^{-6} M excited molecules in a 2 mm cell.)

To estimate the ET rate from donor to excited acceptor, as it is formally described by eq 7, we measured a transient absorption spectrum of dendrimers at a delay of 30 ps following the excitation with 325 nm light. At this delay the majority of excitations reach the acceptor, so the measured spectrum represents the photoinduced optical density changes upon population of the S_1 state of the acceptor. To exclude orientational effects, the measurement was performed in a magic angle configuration. The pump probe spectrum presented in Figure 6 is found to be in good agreement with spectra reported in the literature.^{24–26} It exhibits a bleaching of the spectral region corresponding to the absorption bands of the acceptor as well as photoinduced absorption bands on the blue (below 420 nm) and red (above 690 nm) sides of the spectrum. Because the spectrum of the white light used as a probe did not extend below 390 nm, the changes induced in the 315–405 nm spectral region were measured using a single wavelength probe.

From the data in Figure 6, we estimate a positive differential overlap integral $\Delta J \approx 10^{-14} \text{ M}^{-1} \text{ cm}^{-1} \text{ nm}^4$, which predicts an additional speed up of the ET process. Estimating J^* to be $3.4 \times 10^{14} \text{ M}^{-1} \text{ cm}^{-1} \text{ nm}^4$, the time constant of ET from a donor to an excited acceptor is $k_{\text{ET}}^* = 4.9$ ps, which is nearly half that of the time constant of ET from the donor to the nonexcited acceptor. As shown in eq 5.2, the dynamics of excitations in acceptors are not influenced by the spectral changes in excited acceptors, while the excitation decay in donors, according to eq 5.1, would experience a speeding up at high excitation densities. However, as discussed in the previous section, the absorption bleaching of donors overlaps with the photoinduced absorption of acceptors, so the observations of the donor signal alone are impossible. In addition, the second term in eq 5.1 is comparable with the first one only at high excitation densities, so the donor population dynamics depend only partially on the spectral properties of the excited acceptor.

III.4. ET at High Excitation Density: Experimental Results. Before performing high excitation density experiments, we studied the photodegradation of the dendrimers to estimate the acceptable excitation intensities for the actual experiments.

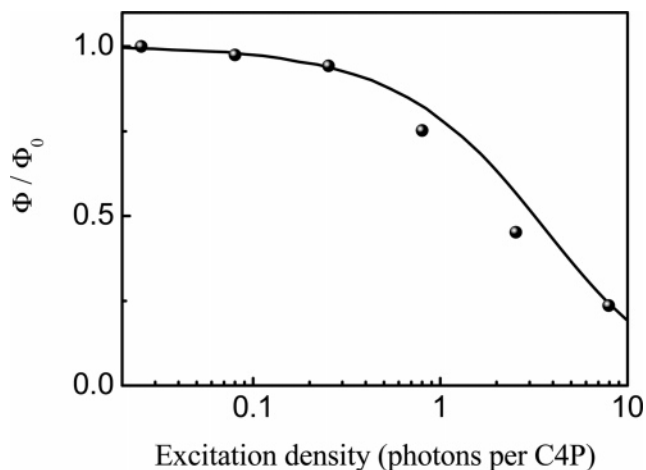


Figure 7. Scaled fluorescence quantum yield of C4P dendrimers versus the excitation density using $\lambda_{\text{ex}} = 325$ nm (dots). The solid line shows a simulation based on eq 8 (for details see text).

The photostability was tested by irradiating a stirred solution of C4P in chloroform at $\lambda_{\text{ex}} = 325$ nm (absorption peak of the donors) or $\lambda_{\text{ex}} = 525$ nm (absorption peak of the acceptors) while monitoring optical density changes (pump–probe signal) at $\lambda_{\text{pr}} = 590$ nm after the 30 ps delay. This test is sensitive to the photodegradation of the donors or the acceptors and to the detachment of the donors from the acceptors. The tests involved absorption of an average of 1000 photons per dendrimer. At low excitation densities (1 photon per 30 dendrimers per pulse absorbed), no observable photodegradation was observed, independent of the excitation wavelength used. At high excitation densities (1 photon per dendrimer per pulse absorbed), excitation in the visible region did not lead to observable photo damage, while UV excitation ($\lambda_{\text{ex}} = 325$ nm) caused photo damage of 50% of the dendrimer molecules after 125 photons per dendrimer were absorbed. This result implies that multiple excitations are responsible for photodamage of the dendrimers. To minimize the influence of photodecomposition on pump–probe data, the experiments at high excitation density conditions were performed while keeping the total number of absorbed photons per single dendrimer molecule below 5, which corresponds to ca. 3% of photodecomposed dendrimers.

Because the determination of the excitation density in absolute units is not straightforward, we have checked the linearity of the number of excited donors with the number of photons per pulse. Because only a single excitation transferred from the donor to the acceptor contributes to the fluorescence, we use the measurement of the dependence of fluorescence quantum yield on the incoming number of photons per pulse for the verification of the excitation density. The ratio between the fluorescence quantum yield at any donor excitation density ϕ to the fluorescence quantum yield in the low excitation density limit, ϕ_0 , can be expressed as

$$\frac{\phi}{\phi_0} = \frac{\sum_{j=1}^4 N_j}{\sum_{j=1}^4 j N_j} \Bigg|_{I=0} \quad (8)$$

where the same approach was used as in the derivation of eq 6. Here we define quantum yield of a chromophore as the number of emitted photons per absorbed photon. In Figure 7, a simulation, obtained by taking into account the number of

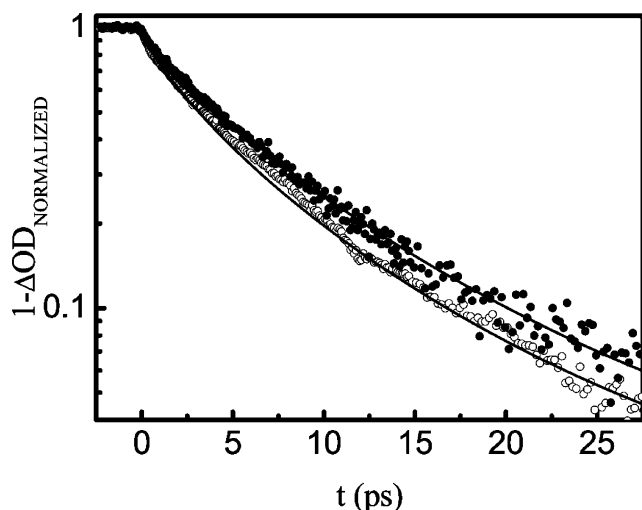


Figure 8. Pump-probe transients measured at $\lambda_{pr} = 590$ nm with excitation densities corresponding to one photon absorbed per 1 dendrimer (open circles) and one photon absorbed per 30 dendrimers (filled circles). Solid lines show the simulated population dynamics obtained using eq 4 (for details see text).

dendrimers with an excited acceptor at various photon fluxes is plotted together with the measured ratio (eq 8). A very good match between the calculated curve and the experimental data demonstrates that effects originating from two-photon absorption by solvent and dendrimers and from the spatial distribution of light intensity do not play a crucial role, validating the absolute excitation densities estimated for the experiments.

Pump-probe transients were measured at excitation densities ranging from 1/100 to 2 photons absorbed per pulse per C4P molecule. The dendrimers were excited at 325 nm, while optical density changes were probed at 590 nm. Typical examples, measured at low (1 photon per 30 C4P molecules absorbed) and high (1 photon per 1 C4P molecule absorbed) excitation densities, are shown in Figure 8. In the case of high excitation densities (1 photon per C4P), the estimated percentages of multiply excited dendrimers with two, three, and four excited donors are 29%, 10%, and 2.5%, respectively. In the case of low excitation densities (1 photon per 30 C4P), less than 2% of excited dendrimers experience multiple excitations. The data clearly show that the formation of the photoinduced acceptor absorption speeds up at high excitation densities, thereby confirming the anticipated acceleration of the ET upon multiple donor excitations. The solid lines in Figure 8 are the calculated formation curves using the model described by eq 4. The modeling was carried out taking into account the effect of variation of the dendrimer geometry on the ET rate. A set of pump-probe traces was calculated for an ensemble of various dendrimer geometries, using a set of k_{ET} and k_{ET}^* values generated using the distribution of donor-acceptor distances with $\sigma = 0.1$ and the effective ET time $k_{eff}^{-1} = 7$ ps calculated previously. Though k_{ET}^* is almost irrelevant in this case, the value estimated in the previous section ($k_{ET}^{*-1} = 4.9$ ps) was used. The solutions acquired were averaged for the ensemble to achieve the dynamics of donor and acceptor populations in a bulk solution. Note that no further fitting procedures were performed after the determination of the effective ET rate and the distribution of donor-acceptor distances. Very good agreement between the measured and the calculated traces suggests reasonable relevance of the model for this system. The determining factor that leads to the increase of the ET rate is the occurrence of the multiple donor excitations in the dendrimer. As discussed in the previous section, the results are

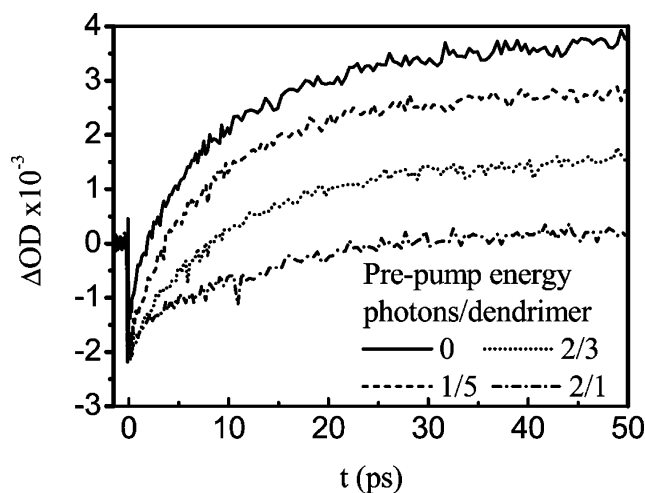


Figure 9. Prepump-pump-probe transients measured at $\lambda_{pr} = 325$ nm for various prepump pulse energies. The prepump polarization is parallel to the pump polarization. The polarization of the probe is set at the magic angle with respect to those of the prepump and pump pulses.

almost independent of the value k_{ET}^* , and we will therefore return to this rate constant using more dedicated experiments in the next section.

III.5. Control of the ET Rate: Prepump-Pump-Probe Experiment. From the previous section, it can be seen that the effect of excitation density on ET dynamics is complex because the ET rate is influenced by multiple factors such as the number of excited donors and changes in spectral response and transition dipole orientation in the excited acceptor. As can be seen from eq 6, with an increase in the number of excited donor molecules, the ET rate should increase independent of the conditions in which the acceptor molecule persists. To separate the effects of the magnitude of the ET rate constant for transfer to the excited state from those due to multiple donor excitations, we performed prepump - pump-probe experiments in which the acceptor is pre-excited to the S_1 state using an intense 550 nm pulse. The delay between prepump and pump pulses should be as short as possible to ensure a fixed orientation and geometry of the dendrimer. However, the solvent needs to relax after the intense prepump pulse, which requires some time. To meet both conditions satisfactorily, the prepump-pump delay was set to 10 ps.

The results of the prepump-pump-probe experiments are shown in Figure 9. In all cases a negative signal corresponding to the photoinduced bleaching induced in donor molecules is observed directly after excitation. With an increase of the delay between the pump and the probe pulses, the signal grows and saturates at a certain positive value. These dynamics are due to the significant photoinduced absorption at 325 nm of the S_1 excited acceptor. The bleaching signal at 325 nm observed at low prepump power and in the conventional pump-probe experiments becomes overshadowed by the photoinduced absorption of the acceptor in the S_1 state resulting from donor-acceptor ET. Eventually, the photoinduced absorption is expected to decay with a time constant of 6.7 ns (lifetime of the S_1 excited state of the acceptor).

Another observation from the data in Figure 9 is that the positive pump-probe signal at longer delays (>30 ps) decreases with increasing prepump pulse energy. This results from the fact that more and more acceptors are already excited upon increasing the prepump energy. Pre-excited acceptors do not contribute to the pump-probe signal even if excitation from

the donors reaches these acceptors because, as discussed above, higher-lying excited states (S_n in Figure 2) are short-lived and the acceptor returns to the S_1 state on a sub-100 fs time scale. In contrast, the initial negative part of the pump–probe signal increases with increasing prepump pulse energy. This originates from the fact that the acceptor has both a weak linear (Figure 1) and a photoinduced (Figure 6) absorption at 325 nm. Because the pre-excitation pulse excites a significant fraction of acceptors, the number of acceptors that contributes to the photoinduced absorption in subsequent pump probe measurements is significantly diminished. This leads to the larger relative contribution of the donor bleaching.

Pre-excitation of the acceptor molecules not only changes the amplitude and sign of the pump–probe signal but indeed also influences the donor–acceptor ET rate. Independent of prepump–pump and probe pulse polarizations, the ET rate is found to decrease with increasing prepump pulse energy. In particular, k_{ET} decreases from ca. 7 ps^{-1} , in the absence of the prepump, to 14 ps^{-1} , when a prepump pulse is applied with an energy corresponding to approximately 2 photons per dendrimer per pulse. This result contradicts the value of k_{ET}^* of 4.9 ps estimated previously. The most likely explanation for the disagreement with the excited-state rate constant estimated from the overlap integral (eq 7) is the difference between the orientations of the $S_0 \rightarrow S_2$ (ET to the acceptor in the ground state) and $S_1 \rightarrow S_n$ (ET to the pre-excited acceptor) transition dipole moments. If these are not parallel, then one should take the relative orientations into account when evaluating the integral in eq 7. Effects of unfavorable donor–acceptor $S_0 \rightarrow S_1$ orientations on the energy transport in dendrimers have previously been observed in single-molecule experiments by Melnikov et al.²⁸ Polarization-selective pump–probe experiments indeed have shown that the relative orientations of the $S_0 \rightarrow S_2$ and $S_1 \rightarrow S_n$ transition dipole moments of the acceptor are close to perpendicular; therefore we expect that the overlap integral is altered severely by the inclusion of a wavelength-dependent orientational factor ($\kappa(\lambda)$), leading to a negative value, and hence to the observed significant “ET blockade”. One interesting consequence of this is that pre-excitation, at least at low excitation densities when no multiply excited dendrimers are present, enables substantial control of the energy transfer rate.

IV. Summary and Conclusions

This paper presented a detailed study of the ET properties of a first generation coumarin–perylene bisimide dendrimer. At low donor excitation intensities fast and efficient (quantum yield ca. 99.5%) donor–acceptor energy transfer is observed. On the basis of a Förster dipole–dipole resonant ET model, the initial energy transfer time constant is estimated to be on the order of 7 ps, which is in good agreement with experimental observations. Frequency-resolved pump–probe measurements reveal a nonexponential behavior of the ET dynamics, which is found to result from variations of the donor–acceptor distances due to conformational disorder. Taking this disorder into account gives an effective ET time constant of 7 ps and a distance distribution with a standard deviation of ca. 10%, consistent with the results of MD simulations.

High pulsed excitation densities lead to more than one excited donor per dendrimer. The simple rate equation model presented here predicts speeding up of the ET with an increase in excitation density arising mainly from the increased number of excited donors per dendrimer. It has been shown by prepump–pump–probe experiments that the ET rate decreases depending

on the number of pre-excited acceptors. The observed decrease is in strong contradiction with the behavior predicted by using the usual overlap integral approach. The origin of this discrepancy lies in the simplicity of calculation of the overlap integral, which does not take the relative transition dipole moment orientations into account. This is a particularly bad approach for C4P dendrimers, because the relevant transition dipole moments ($S_0 \rightarrow S_2$ and $S_1 \rightarrow S_n$) are found to be nearly perpendicular to each other. This causes a sign change of the differential overlap integral and strongly suppresses the ET to the excited acceptor state, i.e., leads to “ET blockade” phenomena.

Acknowledgment. We thank Jasper Knoester for fruitful discussions and Wesley R. Browne for critical reading of this manuscript. This work is part of the research program of the Stichting voor Fundamenteel Onderzoek der Materie, which is financially supported by the Nederlandse Organisatie voor Wetenschappelijk Onderzoek.

References and Notes

- Hecht, S.; Fréchet, J. M. J. *J. Angew. Chem., Int. Ed.* **2001**, *40*, 74.
- Hawker, C. J.; Wooley, K. L.; Fréchet, J. M. J. *J. Chem. Soc., Perkin Trans. 1* **1993**, 1287.
- Mattei, S.; Seiler, P.; Diederich, F.; Gramlich, V. *Helv. Chim. Acta* **1995**, *78*, 1904.
- Jansen, J. F. G. A.; Meijer, E. W.; de Brabander-van den Berg, E. M. M. *J. Am. Chem. Soc.* **1995**, *117*, 4417.
- Liu, M.; Kono, K.; Fréchet, J. M. J. *J. Controlled Release* **2000**, *65*, 121.
- Zeng, F.; Zimmerman, S. C. *Chem. Rev.* **1997**, *97*, 1681.
- Van Heerbeek, R.; Kamer, P. C. J.; Van Leeuwen, P. W. N. M.; Reek, J. N. H. *Chem. Rev.* **2002**, *102*, 3717.
- Twyman, L. J.; King, A. S. H.; Martin, I. K. *Chem. Soc. Rev.* **2002**, *31*, 69.
- Astruc, D.; Chardac, F. *Chem. Rev.* **2001**, *101*, 2991.
- Oosterom, G. E.; Reek, J. N. H.; Kamer, P. C. J.; van Leeuwen, P. W. N. M. *Angew. Chem., Int. Ed.* **2001**, *40*, 1828.
- Tully, D. C.; Fréchet, J. M. J. *Chem. Commun.* **2001**, 1229.
- Tully, D. C.; Wilder, K.; Fréchet, J. M. J.; Trimble, A. R.; Quate, C. F. *Adv. Mater.* **1999**, *11*, 314.
- Tully, D. C.; Trimble, A. R.; Fréchet, J. M. J.; Wilder, K.; Quate, C. F. *Chem. Mater.* **1999**, *11*, 2892.
- Bruinink, C. M.; Nijhuis, C. A.; Peter, M.; Dordi, B.; Crespo-Biel, O.; Auletta, T.; Mulder, A.; Schonherr, H.; Vancso, G. J.; Huskens, J.; Reinhoudt, D. N. C. *Chem.—Eur. J.* **2005**, *11*, 3988.
- Yamamoto, K. *J. Polym. Sci., Part A: Polym. Chem.* **2005**, *43*, 3719.
- Ma, D. G.; Lupton, J. M.; Beavington, R.; Burn, P. L.; Samuel, I. D. W. *Adv. Funct. Mater.* **2002**, *12*, 507.
- Adronov, A.; Fréchet, J. M. J. *Chem. Commun.* **2000**, 1701.
- Kawa, M.; Fréchet, J. M. J. *Chem. Mater.* **1998**, *10*, 286.
- Kawa, M.; Fréchet, J. M. J. *Thin Film Solids* **1998**, *331*, 259.
- Vosch, T.; Cotlet, M.; Hofkens, J.; Van der Biest, K.; Lor, M.; Weston, K.; Tinnefeld, P.; Sauer, M.; Latterini, L.; Müllen, K.; De Schryver, F. C. *J. Phys. Chem. A* **2003**, *107*, 6920.
- Jordens, S.; De Belder, G.; Lor, M.; Schweitzer, G.; Van der Auweraer, M.; Weil, T.; Herrmann, A.; Wiesler, U. M.; Müllen, K.; De Schryver, F. C. *Photochem. Photobiol. Sci.* **2003**, *2*, 1118.
- Fréchet, J. M. J. *J. Polym. Sci., Part A: Polym. Chem.* **2003**, *41*, 3713.
- Wasielewski, M. R. *J. Org. Chem.* **2006**, *71*, 5051.
- Sinks, L. E.; Rybtchinski, B.; Iimura, M.; Jones, B. A.; Goshe, A. J.; Zuo, X.; Tiede, D. M.; Li, X.; Wasielewski, M. R. *Chem. Mater.* **2005**, *17*, 6295.
- Rybtchinski, B.; Sinks, L. E.; Wasielewski, M. R. *J. Am. Chem. Soc.* **2004**, *126*, 12268.
- Kaletas, B. K.; Dobrawa, R.; Sautter, A.; Würthner, F.; Zimine, M.; De Cola, L.; Williams, R. M. *J. Phys. Chem. A* **2004**, *108*, 1900.
- Ahrens, M. J.; Sinks, L. E.; Rybtchinski, B.; Liu, W.; Jones, B. A.; Giaimo, J. M.; Gusev, A. V.; Goshe, A. J.; Tiede, D. M.; Wasielewski, M. R. *J. Am. Chem. Soc.* **2004**, *126*, 8284.
- Melnikov, S. M.; Yeow, E. K. L.; Uji-i, H.; Cotlet, M.; Müllen, K.; De Schryver, F. C.; Enderlein, J.; Hofkens, J. *J. Phys. Chem. B* **2007**, *111*, 708.

- (29) Liu, D.; De Feyter, S.; Cotlet, M.; Stefan, A.; Wiesler, U.-M.; Herrmann, A.; Grebel-Koehler, D.; Qu, J.; Müllen, K.; De Schryver, F. C. *Macromolecules* **2003**, *36*, 5918.
- (30) Gong, L. Z.; Hu, Q. S.; Pu, L. *J. Org. Chem.* **2001**, *66*, 2358.
- (31) Hania, P. R.; Heijs, D. J.; Bowden, T.; Pugžlys, A.; van Esch, J.; Knoester, J.; Duppen, K. *J. Phys. Chem. B* **2004**, *108*, 71.
- (32) Devadoss, C.; Bharathi, P.; Moore, J. S. *J. Am. Chem. Soc.* **1996**, *118*, 9635.
- (33) Grimsdale, A. C.; Vosch, T.; Lor, M.; Cotlet, M.; Habuchi, S.; Hofkens, J.; De Schryver, F. C.; Müllen, K. *J. Lumin.* **2005**, *111*, 239.
- (34) Balzani, V.; Ceroni, P.; Maestri, M.; Vicinelli, V. *Curr. Opin. Chem. Biol.* **2003**, *7*, 657.
- (35) Serin, J. M.; Brousmiche, D. W.; Fréchet, J. M. J. *Chem. Commun.* **2002**, *22*, 2605.
- (36) Cotlet, M.; Vosch, T.; Habuchi, S.; Weil, T.; Müllen, K.; Hofkens, J.; De Schryver, F. C. *J. Am. Chem. Soc.* **2005**, *127*, 9760.
- (37) Cotlet, M.; Gronheid, R.; Habuchi, S.; Stefan, A.; Barbafina, A.; Müllen, K.; Hofkens, J.; De Schryver, F. C. *J. Am. Chem. Soc.* **2003**, *125*, 13609.
- (38) Hahn, U.; Gorka, M.; Vogtle, F.; Vicinelli, V.; Ceroni, P.; Maestri, M.; Balzani, V. *Angew. Chem., Int. Ed.* **2002**, *41*, 3595.
- (39) Hecht, S.; Fréchet, J. M. J. *J. Am. Chem. Soc.* **2001**, *123*, 6959.
- (40) Dichtel, W. R.; Hecht, S.; Fréchet, J. M. J. *Polym. Prepr. (Am. Chem. Soc. Div. Polym. Chem.)* **2002**, *43*, 985.
- (41) Brousmiche, D.; Serin, J. M.; Fréchet, J. M. J.; He, G. S.; Lin, T. C.; Chung, S. J.; Prasad, P. N. *J. Am. Chem. Soc.* **2003**, *125*, 1448.
- (42) He, G. S.; Lin, T. C.; Cui, Y.; Prasad, P. N.; Brousmiche, D.; Serin, J. M.; Fréchet, J. M. J. *Opt. Lett.* **2003**, *28*, 768.
- (43) Neuwahl, F. V. R.; Righini, R.; Adronov, A.; Malenfant, P. R. L.; Fréchet, J. M. J. *J. Phys. Chem. B* **2001**, *105*, 1307.
- (44) Sautter, A.; Kaletas, B. K.; Schmid, D. G.; Dobrawa, R.; Zimine, M.; Jung, G.; van Stokkum, I. H. M.; De Cola, L.; Williams, R. M.; Würthner, F. *J. Am. Chem. Soc.* **2005**, *127*, 6719.
- (45) Würthner, F. *Chem. Commun.* **2004**, 1564.
- (46) Würthner, F.; Sautter, A.; Schmid, D.; Weber, P. J. A. *Chem.—Eur. J.* **2001**, *7*, 894.
- (47) Hurenkamp, J. H.; Browne, W. R.; Augulis, R.; Pugžlys, A.; van Loosdrecht, P. H. M.; van Esch, J. H.; Feringa, B. L. *Org. Biomol. Chem.* **2007**, *5*, 3354.
- (48) Ray, K.; Dutta, A. K.; Misra, T. N. *J. Lumin.* **1997**, *71*, 123.
- (49) Hernando, J.; Hoogenboom, J. P.; van Dijk, E. M. H. P.; Garcia-Lopez, J. J.; Crego-Calama, M.; Reinhoudt, D. N.; van Hulst, N. F.; Garcia-Parajo, M. F. *Phys. Rev. Lett.* **2004**, *93*, 236404.
- (50) Förster, Th. *Ann. Phys.* **1948**, *2*, 55.
- (51) A detailed distribution of both the orientations of the transition dipole moments of the donor and acceptor molecules as well as of the dipole–acceptor distances may be obtained from the MD calculations. In our MD calculations, however, we did not include any solvent molecules and used a rather simple force field model (MM+). We therefore chose to take a more qualitative approach by using average values only rather than detailed distributions.
- (52) Maksimov, M. Z.; Rozman, I. M. *Opt. Spectrosc.* **1961**, *12*, 337.
- (53) Beenken, W. J. D.; Pullerits, T. *J. Chem. Phys.* **2004**, *120*, 2490.
- (54) Wiesenhofer, H.; Beljonne, D.; Scholes, G. D.; Hennebicq, E.; Brédas, J.-L.; Zojer, E. *Adv. Funct. Mater.* **2005**, *15*, 155.
- (55) Beljonne, D.; Cornil, J.; Silbey, R.; Millié, P.; Brédas, J. L. *J. Chem. Phys.* **2000**, *112*, 4749.
- (56) Saini, S.; Singh, H.; Bagchi, B. *J. Chem. Sci.* **2006**, *118*, 23.
- (57) Krueger, B. P.; Scholes, G. D.; Fleming, G. R. *J. Phys. Chem. B* **1998**, *102*, 5378.
- (58) Maus, M.; Mitra, S.; Lor, M.; Hofkens, J.; Weil, T.; Herrmann, A.; Mullen, K.; De Schryver, F. C. *J. Phys. Chem. A* **2001**, *105*, 3961.
- (59) Maus, M.; De, R.; Lor, M.; Weil, T.; Mitra, S.; Wiesler, U. M.; Herrmann, A.; Hofkens, J.; Vosch, T.; Mullen, K.; De Schryver, F. C. *J. Am. Chem. Soc.* **2001**, *123*, 7668.
- (60) Jones, G.; Bergmark, W. R.; Jackson, W. R. *Opt. Commun.* **1984**, *5*, 320.